
**Separation Science and Technology**
Publication details, including instructions for authors and subscription information:
http://www.informaworld.com/smpp/title~content=t713708471

# Theoretical Assessment of Dilute Acetone Removal from Aqueous Streams by Membrane Distillation

Fahmi Abu Al-Rub[a]; Fawzi A. Banat[a]; Mohammad Shannag[a]
[a] DEPARTMENT OF CHEMICAL ENGINEERING, JORDAN UNIVERSITY OF SCIENCE AND TECHNOLOGY, IRBID, JORDAN

Online publication date: 10 December 1999

**To cite this Article** Al-Rub, Fahmi Abu , Banat, Fawzi A. and Shannag, Mohammad(1999) 'Theoretical Assessment of Dilute Acetone Removal from Aqueous Streams by Membrane Distillation', Separation Science and Technology, 34: 14, 2817 — 2836
**To link to this Article: DOI:** 10.1081/SS-100100807
**URL:** http://dx.doi.org/10.1081/SS-100100807

SEPARATION SCIENCE AND TECHNOLOGY, **34**(14), pp. 2817–2836, 1999

# Theoretical Assessment of Dilute Acetone Removal from Aqueous Streams by Membrane Distillation

FAHMI ABU AL-RUB, FAWZI A. BANAT,*
and MOHAMMAD SHANNAG
DEPARTMENT OF CHEMICAL ENGINEERING
JORDAN UNIVERSITY OF SCIENCE AND TECHNOLOGY
IRBID, 22110 JORDAN



## ABSTRACT

The removal of dilute acetone from aqueous streams by air-gap membrane distillation is theoretically assessed. A combined heat and mass transfer model that includes temperature and concentration polarization effects as well as temperature and concentration variation along the module length is employed to predict the flux and selectivity of acetone under the relevant process operating conditions. Three mass transfer solutions are heeded in the model: the exact Stefan–Maxwell, the approximate Stefan–Maxwell, and the Fickian binary solution. Although, behaviorally, the three solutions exhibit the same trends, quantitatively some differences exist between the Fickian-based solution on the one hand and the Stefan–Maxwell solutions on the other hand. The exact and approximate solutions of the Stefan–Maxwell equation showed a similar capability in predicting the process achievement under all process conditions. Predictions showed that acetone selectivity and flux were strongly dependent on feed conditions and air-gap width.

## INTRODUCTION

Fermentation of molasses and other sugar sources was the basis of acetone production when acetone was used for the manufacture of explosive cordite (1). The fermented solvents tend to inhibit microorganism productivity with increasing concentration. For example, the inhibition effect of acetone starts at concentrations beyond 0.5 wt% acetone (2). Therefore, the efficiency of the

* To whom correspondence should be addressed. E-mail: banatf@just.edu.jo

fermentation process can be improved by a continuous removal of the product from fermentation broth while keeping the microorganisms inside.

Several methods have been examined for the continual removal of the inhibitory products from the fermentation broth such as reverse osmosis (3), distillation (4), pervaporation (5–7), and membrane distillation (8). The separation process chosen should minimize thermal, chemical, and mechanical stresses upon the microorganisms. The pervaporation process achieves this requirement and gives high selectivities, but the permeate fluxes are very low. Larrayoz and Puigjaner (5) studied pervaporation of the acetone–water mixture using silicon rubber membranes. At a process temperature of 37°C and a feed concentration of 1.7 to 2.0 wt% acetone, a mass flux of 0.00442 to 0.00088 g/($m^2$·h) and an acetone selectivity of 34 to 39 were observed. Matsumura and Kataoka (6) studied the pervaporation of dilute aqueous butanol and acetone solutions through oleyl alcohol liquid membranes. For the acetone–water mixture, a total flux of 0.04 kg/($m^2$·h) and an acetone selectivity of 160 were observed at a feed concentration of 1 wt% acetone and a temperature of 30°C. Since the permeate fluxes were very low in all pervaporation tests, very large contact areas would be required for the continual removal of the inhibitory products.

In membrane distillation the high mechanical, thermal, or chemical stresses often exerted upon the microorganisms by such competitive processes as reverse osmosis, distillation, and solvent extraction can be avoided. Also, moderate permeate fluxes and selectivities are obtained. Membrane distillation is a combination of thermal and membrane processes in which a hydrophobic porous membrane separates the warmed feed solution from a cooling media. The temperature difference between the two sides of the membrane creates a partial pressure gradient which is responsible for the transmembrane flux. Air-gap membrane distillation (AGMD), the process in which an additional air gap is interposed between the membrane and the condensation surface, is usually recommended for separating surface-active components from water (9).

To the authors' knowledge, the only reported work on dilute acetone removal from aqueous solutions by membrane distillation is by Banat (8). Banat tested only PVDF membranes with a pore size of 0.45 μm. He found that although spontaneous wetting of PVDF membranes outside the cell occurred at a feed concentration exceeding 23 wt% acetone, membrane wetting inside the cell occurred at a lower feed concentration and was strongly dependent upon the feed flow rate. It was also found that PVDF membranes performance degenerated significantly as a function of time and that the experimental results were dramatically affected by membrane deterioration.

In this paper a comprehensive mathematical model that includes all necessary heat, mass, and vapor liquid equilibrium relations is used to examine theoretically the possible use of AGMD in the removal of dilute acetone from





MARCEL DEKKER, INC.
270 Madison Avenue, New York, New York 10016

TABLE 1
Air Gap Module Specifications

| | |
|---|---|
| Module length | 1.0 m |
| Module width | 0.5 m |
| Type of membrane | Flat sheet (Millipore) |
| Membrane material | Polyvinyldene fluoride (PVDF) |
| Pore diameter | 0.45 μm |
| Membrane thickness | 0.11 mm |
| Membrane porosity | 0.75 |
| Membrane tortuosity | 2.0 |
| Cooling plate material | Stainless steel |
| Cooling plate thickness | 2.0 mm |



aqueous streams. The gas-phase acetone–water–air molecular interactions are described by both binary (Fickian) and multicomponent (Stefan–Maxwell) equations. Two solutions of the Stefan–Maxwell equation are considered: the exact matrix solution developed by Krishna and Standart (10, 11) and the approximate solution developed by Krishna and Wesselingh (12). The consonances and differences among the three solutions are discussed along with the process performances under different operating conditions. The predicted results are presented in terms of acetone selectivity and average permeate flux. The simulation results are obtained for a flat-sheet membrane module with the specifications listed in Table 1.

## THEORY

Species transfer in AGMD occurs in a sequence of four steps: movement of the volatile components from the feed bulk to the membrane surface, evaporation at the membrane liquid–gas interface, diffusion through the air-filled pores and the additional air gap, and condensation on a cooling plate. Since the volatility and diffusion rate differ from one component to another, the component which permeates faster would have a lower concentration at the liquid–membrane interface than in the feed bulk. This phenomenon is referred to as concentration polarization (13). Along with the concentration gradient in the boundary layer adjacent to the membrane surface, a temperature gradient also exists. The difference between the feed bulk temperature and the membrane–liquid interface temperature is referred to as temperature polarization (14). Both temperature and concentration polarization are unavoidable phenomena in membrane distillation processes.

Knowledge of the liquid temperature and concentration at the membrane–liquid interface and the condensate–gas interface is necessary to

calculate the vapor composition. According to Banat and Simandl (15), the significance of concentration polarization increases when the target component that preferentially permeates through the membrane is present in the feed at low concentrations. Performing a mass balance on a thin film in the warm feed solution at steady state gives the concentration at the membrane interface (13, 16)

$$x_{im} = x_{ip} - (x_{ip} - x_{ib}) \exp\left[\frac{N_t}{c_t k_{iw}}\right] \tag{1}$$

As derived elsewhere (17), the temperature at the membrane–liquid interface, $T_m$, and at the condensate–gas interface, $T_p$, is

$$T_m = T_b - \frac{U}{h_h}\left((T_b - T_c) + \frac{\sum N_i \lambda_i}{h^*}\right) \tag{2}$$

$$T_p = T_c + \frac{U}{h_c}\left((T_b - T_c) + \frac{\sum N_i \lambda_i}{h^*}\right) \tag{3}$$

where

$$U = \frac{1}{\frac{1}{h_h} + \frac{1}{h_c} + \frac{1}{h^*}} \tag{4}$$

The calculations of the heat transfer coefficients in the hot region, $h_h$, in the cold region, $h_c$, and in the air gap, $h^*$, are detailed elsewhere (17).

The vapor compositions at the evaporating film and condensing film interfaces can be calculated from the phase equilibrium:

$$y_i = \frac{\gamma_i x_i P_i^{\circ}(T)}{P}, \qquad i = 1, 2, \ldots, n-1 \tag{5}$$

The mole fraction of the inert gas at the interface is calculated from the sum of the mole fractions relation:

$$y_n = 1 - \sum_{i=1}^{n-1} y_i \tag{6}$$

Wilson's model is used to calculate $\gamma_i$ and Antoine's equation is used to calculate the saturation vapor pressure, $P_i^{\circ}$ (18).

The temperature, composition, and molar flow rate of the feed solution vary along the feed flow path. The temperature variation occurs as a result of heat loss through conduction and heat supplied for vaporizing the volatile components at the membrane–gas–liquid interface. The variation in composition along the flow path is due to the difference in permeation rates of the transferring components. The temperature of the coolant fluid which flows coun-

tercurrently also varies along the flow path; this is because of the heat gained from the condensing species and the heat transferred by conduction.

Since the molar fluxes are strongly dependent on temperature which varies along the flow path, the flow path is divided into a series of segments (see Fig. 1). The variation of molar flow rate, $m_i^{\mathrm{f}}$, from one segment to another is calculated from a simple mass balance:

$$(m_i^{\mathrm{f}})_{\mathrm{s}+1} = (m_i^{\mathrm{f}})_{\mathrm{s}} - N_i w \Delta L \tag{7}$$

The minus sign indicates that the material is leaving the evaporating film. The variation of bulk feed temperature along the module length is described by

$$(T_{\mathrm{b}})_{\mathrm{s}+1} = \frac{1}{(m_{\mathrm{t}}^{\mathrm{f}})_{\mathrm{s}+1}} \left[ (m_{\mathrm{t}}^{\mathrm{f}} T_{\mathrm{b}})_{\mathrm{s}} - \frac{qw\Delta L}{Cp_{\mathrm{l}}} \right] \tag{8}$$

where $m_{\mathrm{t}}^{\mathrm{f}}$ is the molar flow rate of the liquid feed mixture, $Cp_{\mathrm{l}}$ is the liquid phase specific heat, $T_{\mathrm{b}}$ is the bulk feed temperature, and $q$ is the total energy flux. The minus sign indicates that heat is leaving the feed stream.

Since condensation occurs on an impermeable plate, the flow rate of the cooling water is constant over the flow path. The temperature of the coolant increases once it passes up because heat is transferred from the hot solution to-

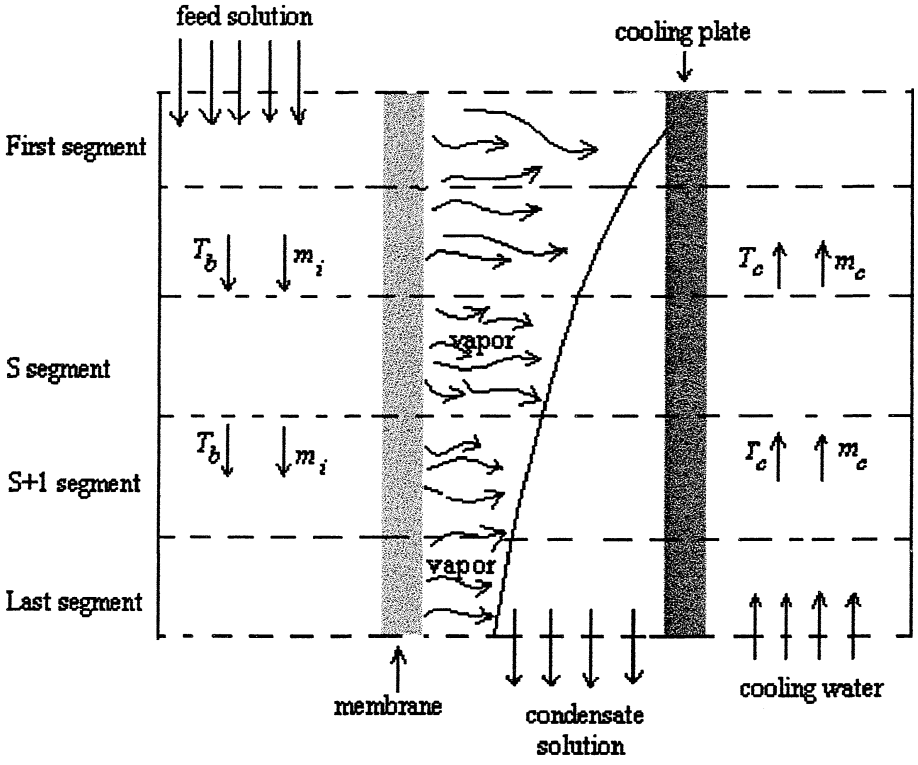


FIG. 1 Segmented air-gap module.





MARCEL DEKKER, INC.
270 Madison Avenue, New York, New York 10016

ward the cooling fluid. The variation of the coolant temperature is described by

$$(T_c)_{s+1} = (T_c)_s - \frac{qw\Delta L}{m_c Cp_c} \tag{9}$$

The minus sign indicates that the coolant liquid and the feed stream are flowing countercurrently. The variation of the condensate flow, $m_i^c$, can be calculated from

$$(m_i^c)_{s+1} = (m_i^c)_s + N_i^x w\Delta L \tag{10}$$

For steady-state transfer $N_i^x$ flux must equal the flux $N_i$ in the vapor phase. Therefore, the average composition of species $i$ in the permeate, $x_{ip}$, is determined by the ratio of the component flux rates as

$$x_{ip} = \frac{\sum_{j=1}^{s} (N_i)_j}{\sum_{j=1}^{s} \left( \sum_{i=1}^{n} N_i \right)_j} \tag{11}$$

For an acetone–water feed mixture, acetone and water vapors pass through the air-filled pores of the membrane and the additional air gap prior to condensation. Therefore, the process is necessarily multicomponent, involving an interaction between three components: water, acetone, and air. Multicomponent separation problems can be solved either by using the Stefan–Maxwell equation or by using the Fickian binary-type equation. The exact solution of the Stefan–Maxwell equation as developed by Krishna and Standart (10, 11) in its general matrix form is

$$(N) = \varepsilon \frac{P}{RT} [\beta][E_m][k_{ym}](y_m - y_p) \tag{12}$$

Note that $\varepsilon$ in Eq. (12) corrects for the effective membrane surface area. The details of the matrix form solution can be found elsewhere (10). The major problem in using the Stefan–Maxwell equations is that the fluxes of species are given implicitly (19). Solving the resulting nonlinear differential equations is tedious (19). To make use of the Stefan–Maxwell equations more accessible, Wesselingh and Krishna (12) suggested the use of the difference approximation method which, as they claimed, can provide an accuracy adequate for many engineering applications. The matrix form solution of the difference approximate technique as suggested by Wesselingh and Krishna (12) is

$$(N) = \varepsilon[H]^{-1}(\Delta y) \tag{13}$$

where the coefficients of the matrix $[H]$ are defined by

$$H_{ii} = -\frac{RT}{P}\sum_{\substack{j=1\\ j\neq i}}^{n}\frac{y_{j,\mathrm{av}}}{k_{ij}} \tag{14}$$

$$H_{ij} = \frac{RT}{P}\frac{y_{i,\mathrm{av}}}{k_{ij}} \tag{15}$$

where $y_{i,\mathrm{av}}$ is the average mole fraction of species $i$. Equation (13) represents a set of linear algebraic equations which can be solved with less mathematical computations than Eq. (12). The mathematical complexities of the Stefan–Maxwell equations have led many investigators to use simpler constitutive relations (binary-type relations). The Fickian approach assumes that the rate of diffusion of species $i$ depends only on its concentration gradient. Consequently, coupling interactions between the diffusing species, which may occur, are neglected. Therefore, the molar fluxes are given by

$$N_i = \frac{\varepsilon P D_{in}}{RT(\delta\tau + b)}\ln\left(\frac{1 - y_{i\mathrm{p}}}{1 - y_{i\mathrm{m}}}\right) \tag{16}$$

After calculating the flux from each segment, the average fluxes may now be estimated as

$$N_{i,\mathrm{av}} = \frac{\int_0^L N_i w dL}{\int_0^L w dL} \tag{17}$$

where $dL$ is the differential segment length.

An iterative computer program was written to calculate the flux and selectivity of the concerned components. The multidimensional Newton–Raphson technique (20) was adopted as an iterative solution procedure to solve the resulting combined heat and mass transfer equations. As the feed stream and the coolant liquid are flowing countercurrently, the temperature variation along the module length must also be solved iteratively in order to match the specified inlet conditions.

## RESULTS AND DISCUSSION

Acetone removal from water via the AGMD process is discussed here in terms of flux and selectivity. Selectivity is the preferential passage of acetone, which can be defined as

$$\alpha_{i\mathrm{w}} = \frac{x_{i\mathrm{p}}/x_{\mathrm{wp}}}{x_{i\mathrm{b}}/x_{\mathrm{wb}}} \tag{18}$$

Higher selectivities lead to a more efficient process if combined with high permeate fluxes. In this section the effect of module length on temperature and concentration variation is discussed along with the effect of the following operating conditions: feed concentration, feed turbulence, feed temperature, coolant turbulence, coolant temperature, and air-gap width.

## Temperature and Concentration Variation along the Module Length

The variation of hot-side and cold-side temperatures along the air-gap module is shown in Fig. 2. Here, the temperature difference is defined as $|T_{in} - T|$, where $T$ is the temperature at a certain module length and $T_{in}$ is the inlet temperature. As shown, the temperature difference of both sides increases along the module length. This is attributed to the fact that the heat required for the evaporation process of a species is supplied from the bulk feed solution while the condensation of diffused species releases heat that transfers through the cooling plate to the cold-side stream. From Fig. 2 it is seen that in-

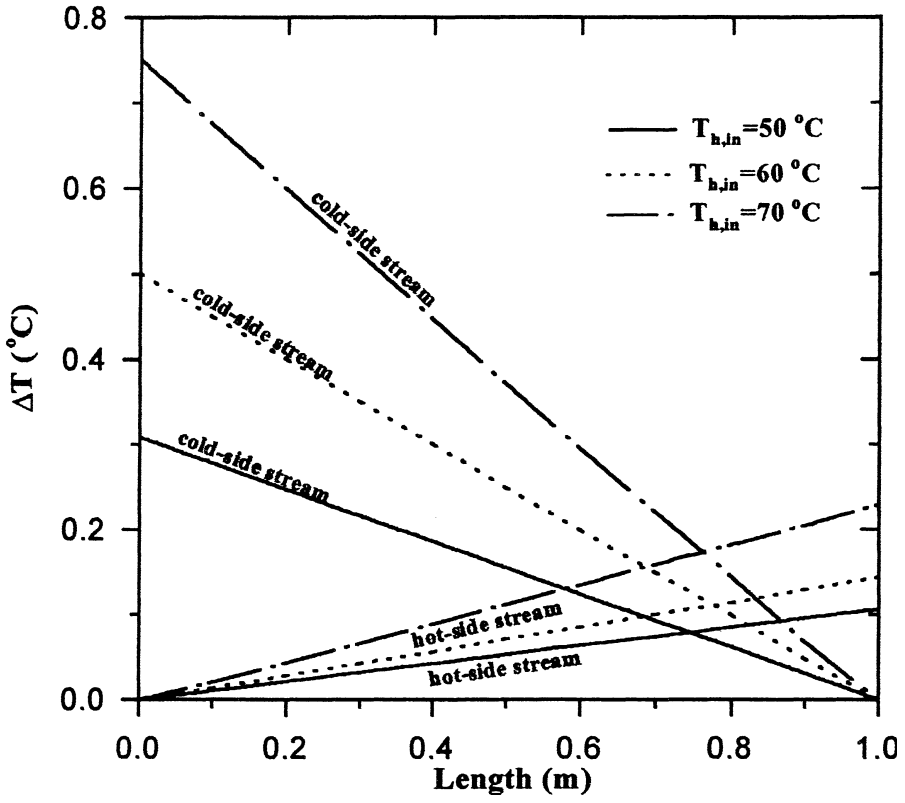


FIG. 2 Effect of module length on temperature difference ($X_{Ain} = 0.15$ wt%, $T_{c,in} = 20$°C, $Re_h = Re_c = 1800$, $b = 0.35$ cm).





MARCEL DEKKER, INC.
270 Madison Avenue, New York, New York 10016

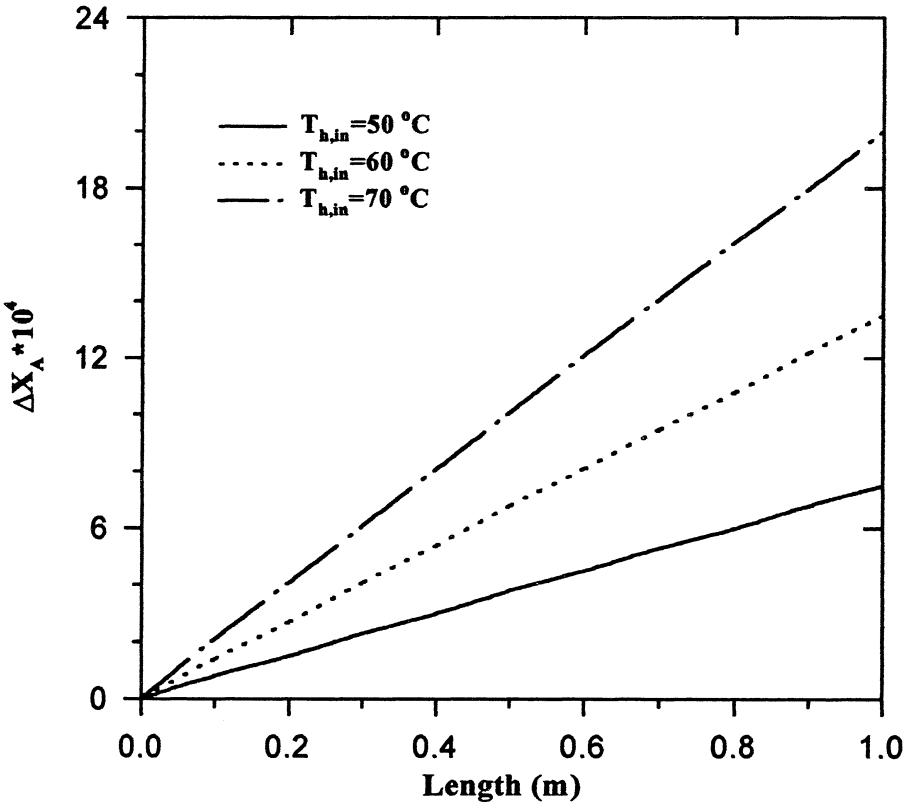


FIG. 3 Effect of module length on concentration difference ($X_{Ain}$ = 0.15 wt%, $T_{c,in}$ = 20°C, $Re_h = Re_c$ = 1800, $b$ = 0.35 cm).

creasing the inlet feed temperature increases the temperature difference. This is due to the increase of the mass transfer driving force with a feed-side temperature increase. Hence, high evaporation and condensation rates are achieved. For example, at 70°C inlet feed temperature, the cold-side temperature increases by 0.75°C while the feed temperature decreases by 0.23°C. For a 0.23°C feed temperature difference, the vapor pressure of water decreases by 2 mmHg, while for acetone it decreases by 8 mmHg. At the cold side, a 0.75°C temperature increase corresponds to a vapor pressure difference of between 1 and 6 mmHg. Therefore, for short modules, it is safe to neglect temperature variation along the module length.

The effect of inlet feed temperature on concentration variation along the module length is shown in Fig. 3. As shown, the concentration difference increases as the feed temperature increases. This is mainly attributed to the increase of flux due to temperature increase. However, as noted, the variation in concentration is marginal.

## Effect of Operating Variables on Permeate Flux and Selectivity

In this section the effect of key operating variables on permeate flux and acetone selectivity is examined.

### *Effect of Acetone Feed Concentration*

Figure 4 shows the effect of acetone concentration on flux and selectivity. It is clear that the flux of acetone increases in approximately a linear relation with feed composition while the water flux is nearly constant. This dependency is a reflection of the vapor–liquid equilibrium relations. It can also be seen that as the acetone concentration increases, the selectivity first increases, reaches a maximum, and then decreases slightly. Increasing the concentration of acetone in the feed mixture steadily increases its concentration in the permeated flux. The presence of a "maximum" in Fig. 4 stems only from the mathematical definition of selectivity (Eq. 18). A similar behavior was noticed by Gostoli and Sarti (9) in separating ethanol from a dilute ethanol–water mixture. They noticed that ethanol selectivity was highly sensitive to the feed composition, and they concluded that the membrane distillation process

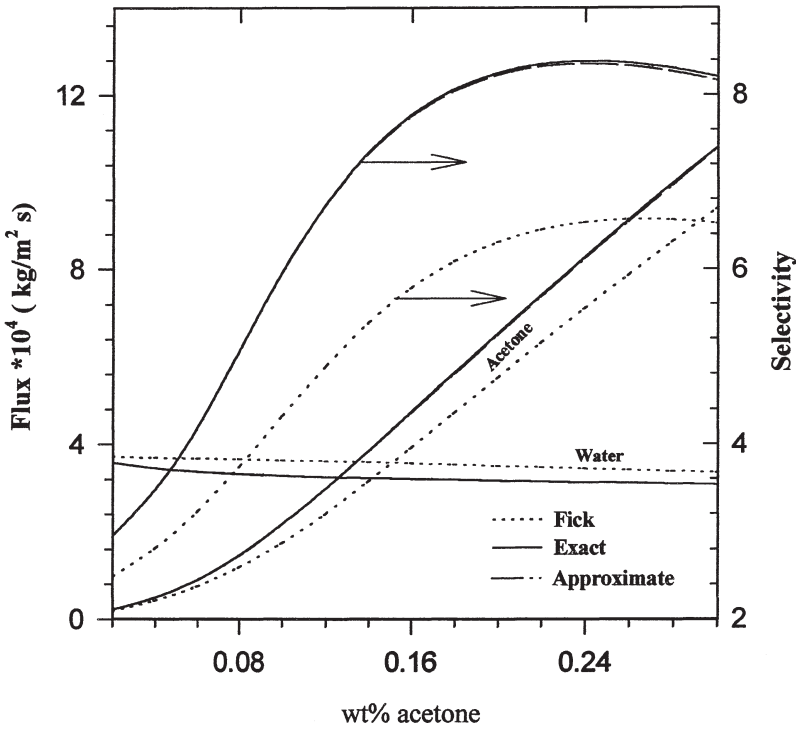


FIG. 4 Effect of feed concentration on the flux and selectivity of acetone ($T_h$ = 50°C, $T_c$ = 20°C, $Re_h = Re_c$ = 1800, $b$ = 0.35 cm).

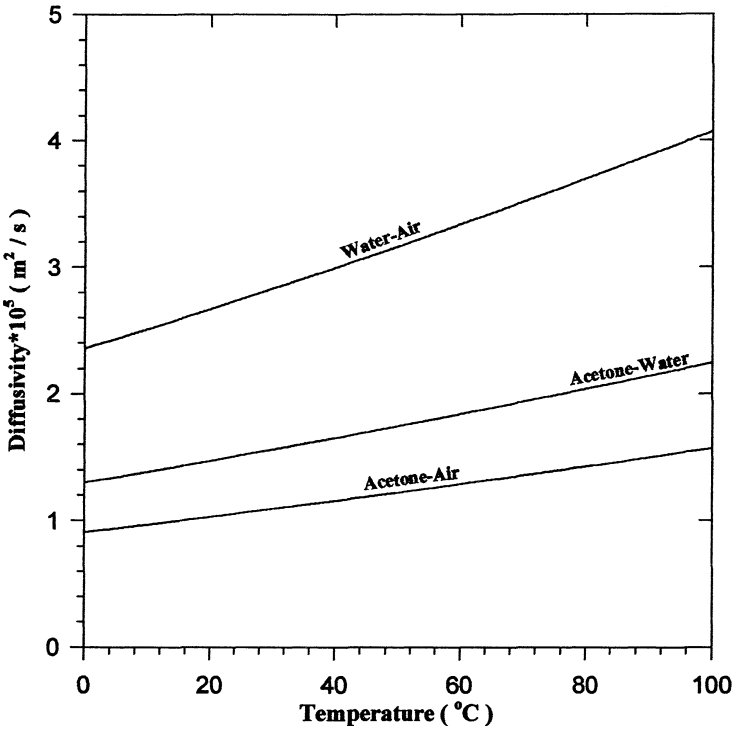


FIG. 5 Effect of temperature on vapor-phase diffusivities.

is ethanol selective for a low ethanol content in the feed but becomes water selective for a high ethanol content.

The predicted curves of the Fickian, exact, and approximate Stefan–Maxwell methods are shown in Fig. 4. It is clear that the results of the difference approximate method are the same as the results of the exact method. This is attributable to two reasons:

- The gap space is mainly composed of trapped air since its solubility in the condensate film is negligible. Therefore, the air component will be present in a large excess and the two other component, acetone and water, will be present in small amounts.
- The approximate method takes all possible coupling interactions into account, the same as for the exact Stefan–Maxwell method.

As shown in Fig. 4, the flux of water and acetone predicted by the Fickian method is greater and less, respectively, than the corresponding predicted values by the Stefan–Maxwell methods. This behavior is reflected in the predicted selectivity. The acetone selectivity predicted by the Stefan–Maxwell approaches is greater than that predicted by the Fickian method. To explain this, consider the binary diffusivities shown in Fig. 5: The diffusivity of the acetone-water vapor mixture is greater than the acetone–air diffusivity and

less than the water–air diffusivity. In the Fickian approach, only the acetone–air and water–air diffusivities are needed. The flux of both acetone and water is independent of the acetone–water interactions in the Fickian approach, while the acetone–water interactions play an important role in flux prediction when using the Stefan–Maxwell methods.

### *Effect of Hot Feed Temperature*

Figure 6 shows the effect of hot-side temperature on the predicted flux of acetone at constant feed concentration. It is clear that the flux increases exponentially with temperature increase. This is attributed to the exponential dependency of acetone vapor pressure on temperature. Shown in Fig. 6 is the effect of feed temperature on acetone selectivity. According to the simulation results, the preferential passage of the volatile component increases until a maximum is reached. After that, more heating of the feed solution leads to a worsening in process performance. The "nonintuitive" selectivity maximum results from the negative effect of flux increase on concentration and temperature polarization. The impact of mass flux increase associated with temperature rise on the phenomenon of concentration polarization can be elucidated from Eq. (1). According to Eq. (1), when the flux is very low, the concentrations of acetone at the membrane interface and in the liquid bulk will be ap-

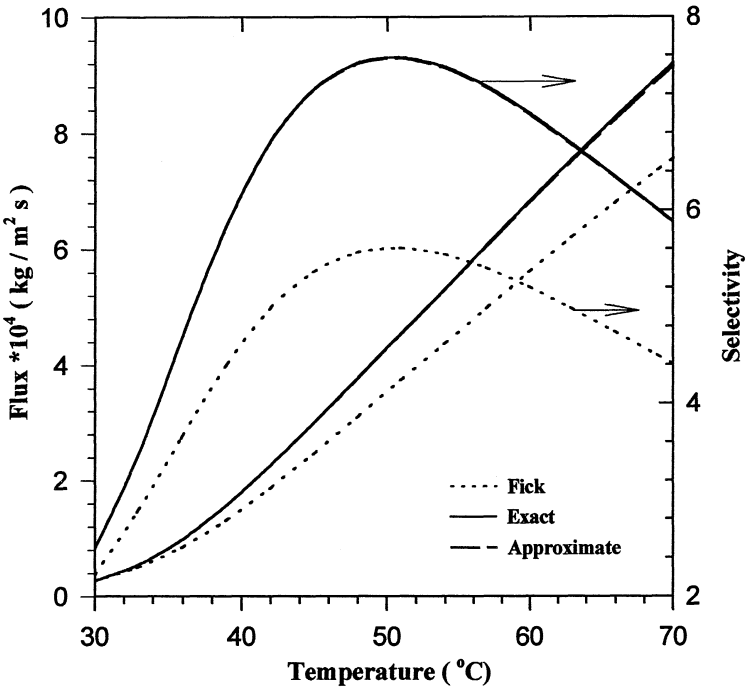


FIG. 6 Effect of feed temperature on the flux and selectivity of acetone ($X_A$ = 0.15 wt%, $T_c$ = 20°C, $Re_h = Re_c$ = 1800, $b$ = 0.35 cm).

proximately the same. However, if the flux is increased, the concentration drop at the membrane interface will consequently be increased. Moreover, the flux increase with temperature rise requires more heat of vaporization. Because heat is withdrawn from the feed to vaporize the permeate, a higher flux increases the temperature polarization effect. Therefore, the progressive increase of the effects of temperature and concentration polarization with a temperature rise is the cause of a selectivity decrease.

As shown in Fig. 6, the difference approximate Stefan–Maxwell method provides the same results as the exact method. The Fickian approach performs well if the feed temperature is low while its results differ noticeably from the exact results at high temperatures. This is due to neglecting the diffusional interactions of acetone–water whose effects are more pronounced at high temperatures. The effect of acetone–water interactions appears through the cross mass transfer coefficients. These cross coefficients are functions of binary diffusivities and vapor composition. The low flux mass transfer coefficients were corrected to be applicable for finite flux. These correction coefficients are function of molar flux, binary diffusivities, diffusion path length, and average temperature. Since binary diffusivities, vapor composition, and molar flux increase with increasing feed temperature, the magnitude of the cross finite mass transfer coefficients also increase. This leads to a large difference between the "Fickian" and the "exact" curves at high feed temperatures.



### *Effect of Cold-Side Temperature*

Figures 7 and 8 show the effect of the coolant temperature on flux and selectivity. As shown in Fig. 7, the flux decreases steadily with cooling temperature increase. With a molar fluxes decrease, the correction factor for low flux mass transfer coefficients also decreases. Therefore, as the coolant temperature increases, the fluxes predicted by the Stefan–Maxwell approaches become closer to the corresponding values predicted by the noninteracting Fickian approach. The increase in the acetone vapor pressure with temperature is greater than that of water. Therefore, the decrease in the mass transfer driving force of acetone is greater than that of water. This is reflected by the decrease in acetone selectivity seen in Fig. 8.

### *Effect of Hydrodynamic Conditions*

The ratio between the concentration of the more volatile component at the vapor–liquid interface and in the bulk feed can be maximized in different ways (8); one of them is by increasing the mass transfer coefficient. The mass transfer coefficient depends strongly on the hydrodynamics of the system. In this section, both feed and coolant turbulence were varied at fixed hot- and cold-side temperatures in order to reduce both concentration and temperature polarizations.



MARCEL DEKKER, INC.
270 Madison Avenue, New York, New York 10016

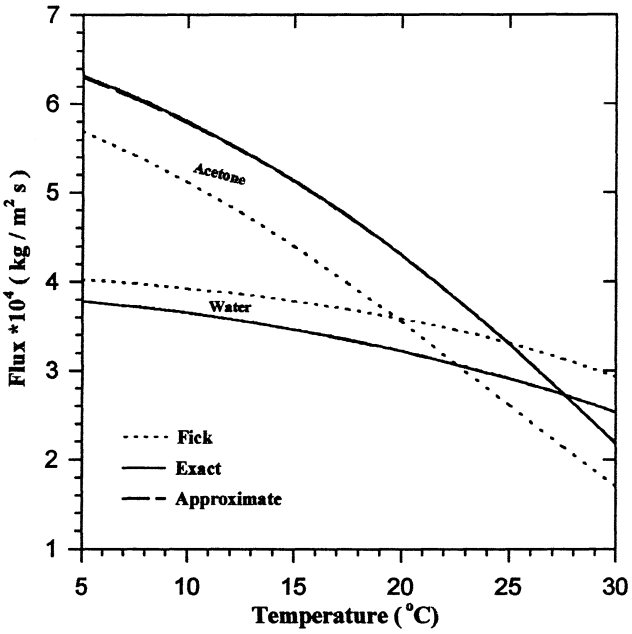


FIG. 7 Effect of coolant temperature on flux ($X_A = 0.15$ wt%, $T_h = 50°C$, $Re_h = Re_c = 1800$, $b = 0.35$ cm).

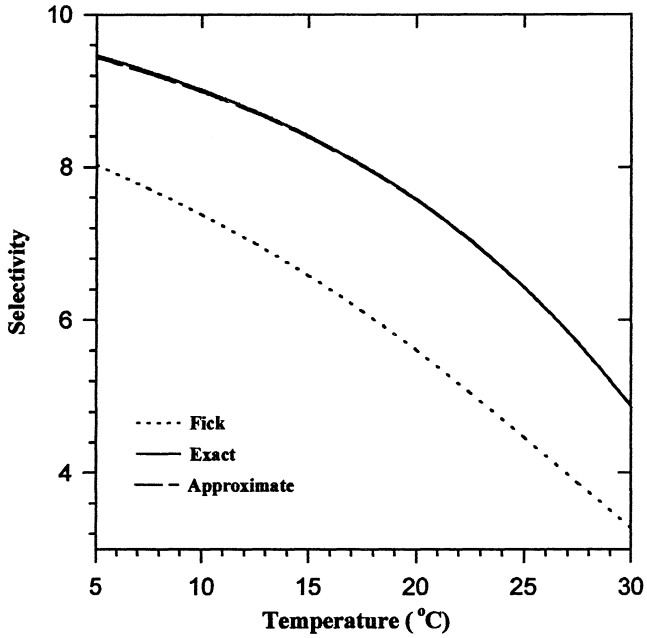


FIG. 8 Effect of coolant temperature on selectivity ($X_A = 0.15$ wt%, $T_h = 50°C$, $Re_h = Re_c = 1800$, $b = 0.35$ cm).





MARCEL DEKKER, INC.
270 Madison Avenue, New York, New York 10016

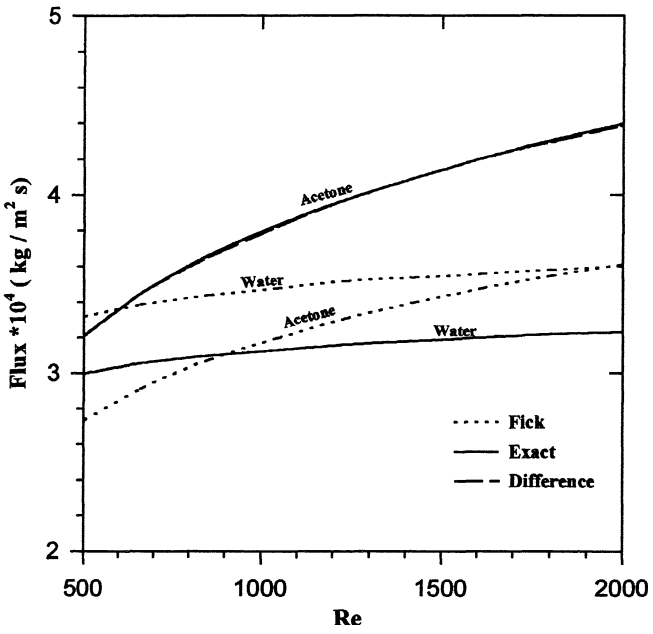


FIG. 9 Effect of feed Reynolds number on flux ($X_A = 0.15$ wt%, $T_h = 50°C$, $T_c = 20°C$, $Re_c = 1800$, $b = 0.35$ cm).

The effect of hydrodynamic conditions on flux and selectivity at the feed side of a membrane is given in Figs. 9 and 10. It can be observed in both figures that the flux and selectivity decrease when the Reynolds number decreases. This is due to a decrease of the mass transfer coefficient with a Reynolds number decrease.

When the coolant turbulence increases, the effect of temperature polarization decreases, and as a consequence the selectivity and the flux increase as shown in Fig. 11. However, since the vapor pressure changes slightly at low temperature levels, the flux and selectivity are more strongly influenced by the Reynolds number at the feed side than by the Reynolds number at the cold side.

The contribution of hydrodynamic conditions in raising acetone–water interactions is very small. This is due to the small change of diffusivities, vapor composition, and average temperature with the hydrodynamic conditions. Therefore, nearly constant differences between the Stefan–Maxwell predictions and the corresponding Fickian prediction were noticed.

### *Effect of Air-Gap Width*

The predicted effect of air-gap width on flux and selectivity is shown in Fig. 12. The permeate flux is inversely proportional to the gap width. By increasing the air-gap width, the acetone and water fluxes predicted by the Stefan–-

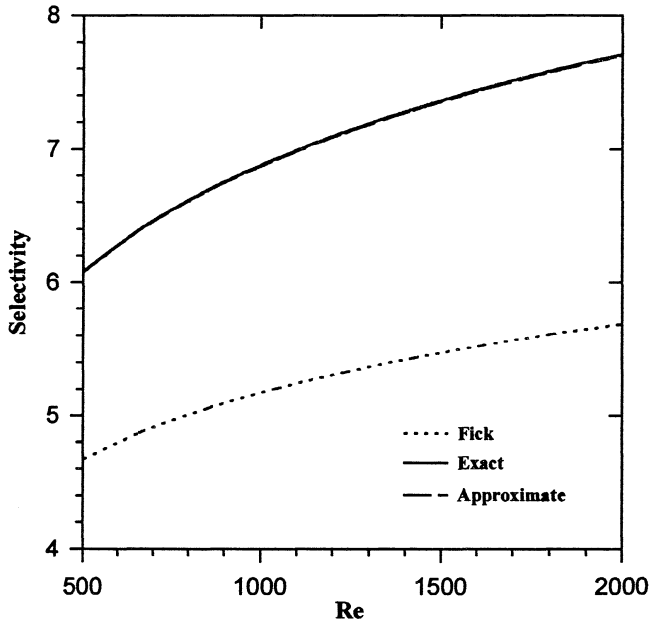


FIG. 10 Effect of feed Reynolds number on selectivity ($X_A$ = 0.15 wt%, $T_h$ = 50°C, $T_c$ = 20°C, $Re_c$ = 1800, $b$ = 0.35 cm).

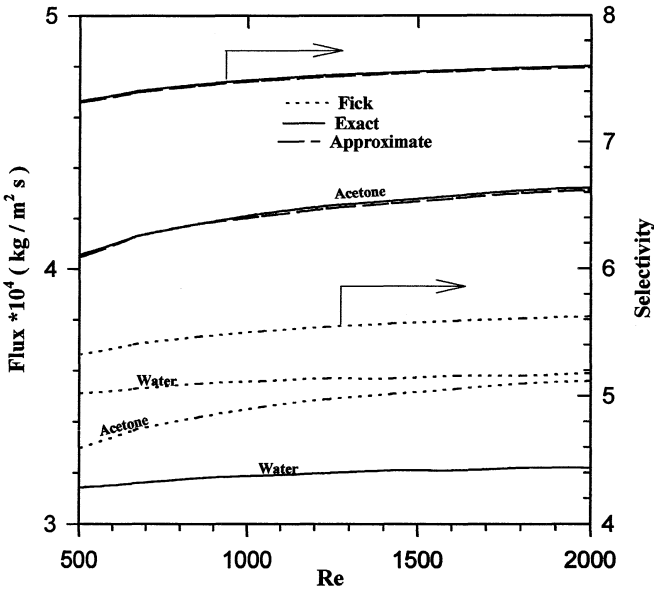


FIG. 11 Effect of coolant Reynolds number on the flux and selectivity of acetone ($X_A$ = 0.15 wt%, $T_h$ = 50°C, $T_c$ = 20°C, $Re_h$ = 1800, $b$ = 0.35 cm).





MARCEL DEKKER, INC.
270 Madison Avenue, New York, New York 10016

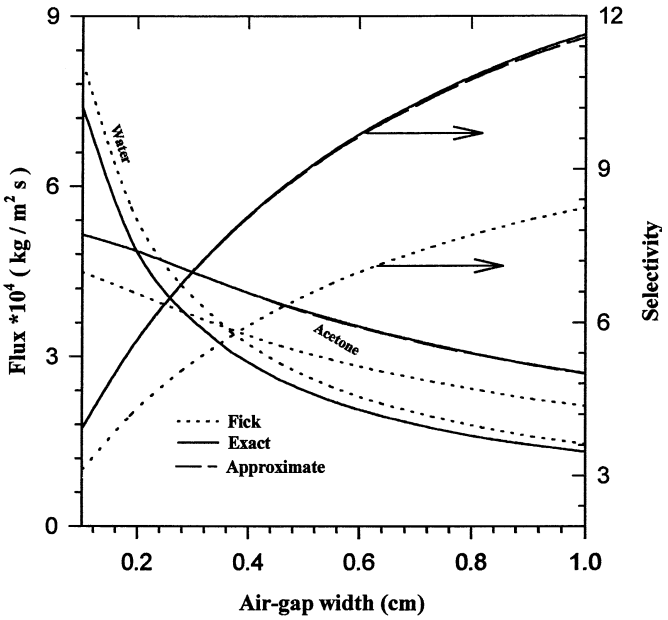


FIG. 12 Effect of air-gap width on the flux and selectivity of acetone ($X_A$ = 0.15 wt%, $T_h$ = 50°C, $T_c$ = 20°C, $Re_h = Re_c$ = 1800).

Maxwell methods move closer to the Fickian predictions. This is due to the decrease in correction factors for zero flux mass transfer coefficients. It is also predicted that increasing the air-gap width will increase the selectivity. This is mainly due to the reduced effect of flux on concentration and temperature polarizations. However, since the process is judged on both flux and selectivity, selectivity increase at the expense of flux decrease is not necessarily a process improvement.

## CONCLUSIONS

A comprehensive theoretical model was developed and numerically solved to predict the performance of air-gap membrane distillation in the removal of dilute acetone concentrations from aqueous streams. The exact and approximate Stefan–Maxwell equation solutions along with the binary Fickian solution were considered in the model. The model takes into account temperature and concentration variations along the diffusion and flow paths. An effort was made to highlight the effects of the various process operating key parameters on acetone flux and selectivity. The approximate and exact solution of the Stefan–Maxwell equation showed similar capabilities in predicting the process performance, albeit less computational efforts were required in the approximate technique. The Fickian solution showed the same trends as did the Stefan–Maxwell solutions; however, some quantitative differences exists among

them. The acetone flux and selectivity were more dependent on the feed-side temperature and hydrodynamic conditions than on the cold-side conditions. The location of optimum acetone selectivity was dependent on feed temperature and composition. The rise in acetone selectivity achieved by widening the air-gap width was offset by acetone flux reduction. The model thus provides insight into the significance of gaseous molecular interactions and could be used for further process development.

## NOTATION

| | |
|---|---|
| $b$ | air-gap thickness (m) |
| $c$ | molar concentration (mol/m$^3$) |
| $Cp_l$ | specific heat (J/mol·K) |
| $D$ | vapor-phase diffusivity (m$^2$/s) |
| [E] | matrix of high flux correction factors |
| $h$ | heat transfer coefficient (W/m$^2$·K) |
| [$H$] | matrix defined by Eqs. (13) and (14) |
| $k$ | mass transfer coefficient (m/s) |
| [$k_y$] | matrix of zero flux mass transfer coefficients (m/s) |
| $L$ | membrane length (m) |
| $m$ | molar flow rate (mol/s) |
| $N$ | molar flux (mol/m$^2$·s) |
| ($N$) | molar flux column matrix |
| $P$ | total pressure (Pa) |
| $P°$ | vapor pressure (Pa) |
| $q$ | heat flux (W/m$^2$) |
| $R$ | universal gas constant (J/mol·K) |
| $T$ | absolute temperature (K) |
| $U$ | overall heat transfer coefficient (W/m$^2$·K) |
| $w$ | membrane width (m) |
| $x$ | mole fraction in the liquid phase |
| $X$ | mass fraction in the liquid phase |
| $y$ | mole fraction in the vapor phase |

### *Greek Symbols*

| | |
|---|---|
| $\alpha$ | selectivity |
| [$\beta$] | matrix in Eq. (11) |
| $\gamma$ | activity coefficient |
| $\delta$ | membrane thickness (m) |
| $\varepsilon$ | porosity |
| $\lambda$ | latent heat of vaporization (J/mol) |
| $\tau$ | tortuosity |





MARCEL DEKKER, INC.
270 Madison Avenue, New York, New York 10016

### *Subscripts and Superscripts*

| | |
|---|---|
| av | average |
| b | bulk |
| c | cooling plate |
| f | feed |
| h | hot region |
| *i*, *j*, *k*, *n* | indexes denoting component number |
| m | membrane |
| p | cooling plate side |
| s | segment index |
| t | total |
| w | water |
| x | liquid phase |
| * | air-gap region |



## REFERENCES


1. J. A. Monick, *Alcohols*, Reinhold, New York, NY, 1968.
2. A. Friedel, N. Qureshi, and S. Madox, "Continuous Acetone–Butanol–Ethanol (ABE) Fermentation Using Immobilized Cells of *Clostridium acetobutylicum* in a Packed Reactor and Integration with Product Removal by Pervaporation," *Biotechnol. Bioeng.*, *38*, 518–527 (1991).
3. A. Garcia, E. L. Iannotti, and J. L. Fischer, "Butanol Fermentation: Liquor Production and Separation by Reverse Osmosis," *Ibid.*, *28*, 785–791 (1986).
4. A. Ramalingham and R. K. Finn, "The Vacuferm Process, a New Approach to Fermentation of Alcohols," *Ibid.*, *19*, 583–589 (1977).
5. M. A. Larrayoz and L. Puigjaner, "Study of Butanol Extraction through Pervaporation in Acetobutylic Fermentation," *Ibid.*, *30*, 692–696 (1987).
6. M. Matsumura and H. Kataoka, "Separation of Dilute Aqueous Butanol and Acetone Solution by Pervaporation through Liquid Membrane," *Ibid.*, *30*, 887–895 (1987).
7. M. E. Hollein, M. Hammond, and C. S. Slater, "Concentration of Dilute Acetone–Water Solutions Using Pervaporation," *Sep. Sci. Technol.*, *28*, 1043–1061 (1993).
8. F. A. Banat, "Membrane Distillation for Removal of Volatile Organic Compounds from Water," Ph.D. Thesis, McGill University, Canada, 1994.
9. C. Gostoli and G. C. Sarti, "Separation of Liquid Mixtures by Membrane Distillation," *J. Membr. Sci.*, *41*, 211–224 (1989).
10. R. Krishna and G. L. Standart, "A Multicomponent Film Model Incorporating an Exact Matrix Method of Solution to the Maxwell–Stefan Equations," *AIChE J.*, *22*, 383–389 (1976).
11. R. Krishna and G. L. Standart, "Mass and Energy Transfer in Multicomponent Systems," *Chem. Eng. Commun.*, *3*, 201–275 (1979).
12. J. A. Wesselingh and R. Krishna, *Mass Transfer*, Ellis Horwood, Chichester, England, 1990.
13. R. Psaume, Ph. Aptel, Y. Aurelle, J. C. Mora, and J. L. Bersillon, "Pervaporation: Importance of Concentration Polarization in the Extraction of Trace Organics from Water," *J. Membr. Sci.*, *36*, 373–384 (1988).




MARCEL DEKKER, INC.
270 Madison Avenue, New York, New York 10016

14. L. Martinez-Diez and M. Vazquez-Conzalez, "Temperature Polarization in Mass Transport through Hydrophobic Porous Membranes," *AIChE*, *42*, 1844–1852 (1996).
15. F. Banat and J. Simandl, "Removal of Benzene Traces from Contaminated Water by Vacuum Membrane Distillation," *Chem. Eng. Sci.*, *51*, 1257–1265 (1996).
16. M. Belkacem, D. Hadjiev, and Y. Aurelle, "A Model for Calculations of the Steady State Flux of Organic Ultrafiltration Membranes for the Case of Cutting Oil Emulsions," *Chem. Eng. J.*, *56*, 27–32 (1995).
17. F. A. Banat and J. Simandl, "Desalination by Membrane Distillation: A Parametric Study," *Sep. Sci. Technol.*, *33*, 201–226 (1998).
18. J. Gmehling and U. Onken, *Chemistry Data Series, Vol. 1* (*Parts 1–10*), *Vapor–Liquid Equilibrium Data Collection*, Dechema, Frankfurt, 1977.
19. J. A. Wesselingh, "How on Earth Can I Get Chemical Engineers to Do Their Multicomponent Mass Transfer Sums Properly," *J. Membr. Sci.*, *73*, 323–333 (1992).
20. C. F. Gerald and P. O. Wheatley, *Applied Numerical Analysis*, 3rd ed., Addison-Wesley, Reading, MA, 1984.

*Received by editor July 28, 1998*
*Revision received February 1999*

# Request Permission or Order Reprints Instantly!